ADVANCED FUNCTIONAL MATERIALS
www.afm-journal.de

Highly Stable Nanoporous Sulfur-Bridged Covalent Organic Polymers for Carbon Dioxide Removal

Hasmukh A. Patel, Ferdi Karadas, Jeehye Byun, Joonho Park, Erhan Deniz, Ali Canlier, Yousung Jung, Mert Atilhan,* and Cafer T. Yavuz**

Carbon dioxide capture and separation requires robust solids that can stand harsh environments where a hot mixture of gases is often found. Herein, the first and comprehensive syntheses of porous sulfur-bridged covalent organic polymers (COPs) and their application for carbon dioxide capture in warm conditions and a wide range of pressures (0–200 bar) are reported. These COPs can store up to 3294 mg g^{-1} of carbon dioxide at 318 K and 200 bar while being highly stable against heating up to 400 °C. The carbon dioxide capacity of the COPs is also not hindered upon boiling in water for at least one week. Physisorptive binding is prevalent with isosteric heat of adsorptions around 24 kJ mol^{-1}. M06–2X and RIMP2 calculations yield the same relative trend of binding energies, where, interestingly, the dimer of triazine and benzene play a cooperative role for a stronger binding of CO_2 (19.2 kJ mol^{-1}) as compared to a separate binding with triazine (13.3 kJ mol^{-1}) or benzene (11.8 kJ mol^{-1}).

1. Introduction

Developments in the highly porous organic frameworks with nanometer-scale porosity (1–100 nm) have attracted significant attention due to their wide range of potential applications which includes sorption and separation of gases, catalysis, removal of hazardous compounds, water treatment, support for catalytically active species, and electronic devices.[1–4] Carbon dioxide (CO_2) removal from the flue gas by porous materials is a key step in CO_2 sequestration for preventing global warming. Developing porous materials which stores and releases CO_2 with fast kinetics and high reversibility over multiple cycles is of widely discussed strategy for a viable adsorption process in CO_2 separation.[5,6] Several porous materials such as mesoporous silica, layered materials, zeolites, activated carbon, metal–organic frameworks (MOFs), covalent organic frameworks (COFs), and porous polymers with excellent CO_2 adsorption capacities have been reported.[7] Among them, MOFs, COFs, and porous polymers gained substantial attention due to their high surface area, ability to be functionalized, thermal stability, recyclability, and selectivity for CO_2 over other gases.[2,8–12]

The CO_2 sorption on adsorbents is mainly governed by physisorption and chemisorption phenomena. A facile reversibility and lower selectivity of CO_2 at low pressures is the characteristic of physisorption, while higher selectivities and capacities but low reversibility observed in chemisorbing materials such as amine functionalized inorganic or organic materials.[13] Although, MOFs are recognized for higher adsorption capacity for CO_2, the oxidation and hydrolysis of MOFs due to the dative nature of the metal–ligand bonds restricts their application in humid conditions. Moreover, CO_2 adsorption capacity does not only dependent on the microporous surface area but sufficient level of functionalities which tune the isosteric heat of adsorption required to attain higher CO_2 adsorption capacity.[14] Among the highest surface area porous polymers, porous polymer networks (PPN–4)[15] and diamond-like porous aromatic frameworks (PAF–1)[16] demonstrated specific surface area of 6461 and 5640 m^2 g^{-1} respectively. CO_2 adsorption capacity of PPN–4 and PAF–1 is 1710 mg g^{-1} (295 K, 50 bar) and 1300 mg g^{-1} (273 K, 40 bar). A possible advantage of porous polymers, compared to other microporous materials such as zeolites and activated carbons, is the potential synthetic diversity that can be incorporated into these organic structures. For example, hydroxyl terminated polymeric organic frameworks (POF) show high surface area, low energy band gap with CO_2 adsorption capacity of 185 mg g^{-1} at 1 bar and 273 K.[17] Porous organics containing nitrogen in the backbone provide excellent selectivity of CO_2 over nitrogen as much as 442 calculated by ideal adsorbed solution theory (IAST) at 295 K.[18] Commercially useful amorphous materials, such as activated carbons, have long been demonstrated that crystalline order is not a prerequisite for gas capture, and it was established that amorphous organic microporous materials can be prepared as simple as formation of a hyper cross-linked polymer (HCP) network.[19,20] Interestingly, many HCPs can be dissolved in common solvents and their ability to form film makes them ideal porous polymers for membrane based applications.[21,22] In all these porous polymers, however, the use of costly catalysts, lengthy synthesis, and lack of

Dr. H. A. Patel, J. Byun, Dr. J. Park, Dr. A. Canlier, Prof. Y. Jung, Prof. C. T. Yavuz
Graduate School of EEWS
Korea Advanced Institute of Science and Technology (KAIST)
Daejeon 305–701, Republic of Korea
E-mail: ysjn@kaist.ac.kr; yavuz@kaist.ac.kr
Dr. F. Karadas, Dr. E. Deniz, Prof. M. Atilhan
Department of Chemical Engineering
Qatar University
2713 Doha, Qatar
E-mail: mert.atilhan@qu.edu.qa

DOI: 10.1002/adfm.201202442

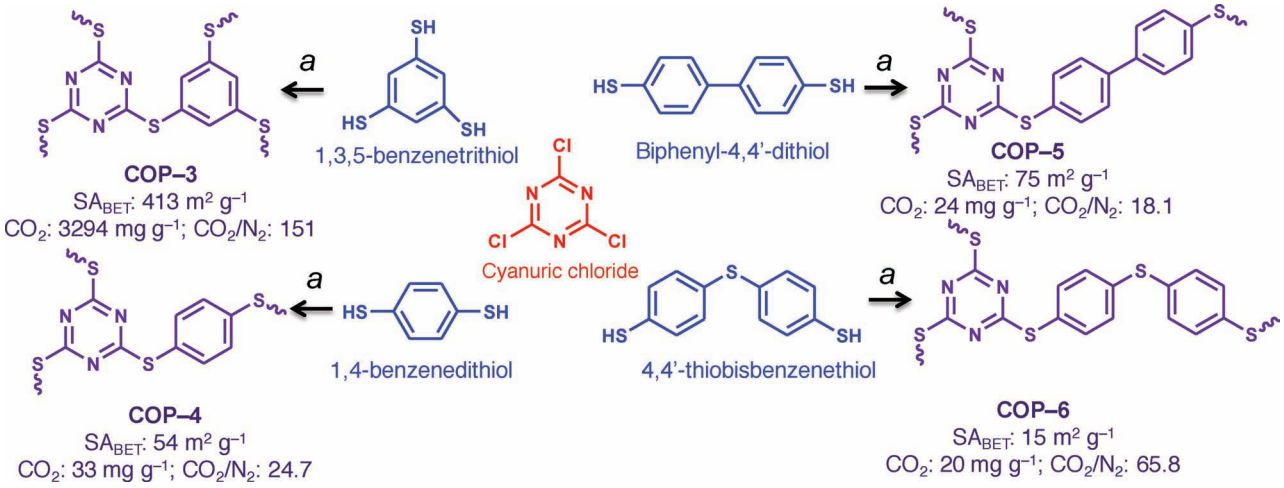

Scheme 1. Chemical structures and properties of sulfur bridged COPs where appropriate thiol linkers are attached to triazine cores. a: dioxane, 85 °C and DIPEA, SA_{BET}: BET surface area, CO_2 adsorption measured at 318 K and 200 bar for COP–3, and at 273 K and 1 bar for COPs–4–6. CO_2/N_2 (0.15:0.85) selectivity by IAST.

stability or chemical versatility causes significant drawbacks when large scale industrial operations are in question.

Triazines feature high nitrogen content as well as multidentate chemistry, a necessity when a network polymer with permanent porosity is desired.[12] A reactive triazine derivative, cyanuric chloride is an attractive molecule for various organic syntheses owing to its low cost and chemo- and thermo-selective reactivity. The generally accepted reactivity trend includes a first substitution at 273 K, the second at 298 K and the third at more than 343 K.[23] A series of triazine based mesoporous graphitic carbon nitride structures with exceptional thermal stability and permanent porosity are developed by Thomas et al.[24–26] Porous aromatic framework based on cyanuric chloride and piperazine with moderate surface area as control drug release carrier is reported.[27]

Herein, we report a facile, catalyst free, low temperature synthesis of sulfur based covalent organic polymers (COPs) which primarily contains triazine moiety as basic building block with surface areas up to 413 m^2 g^{-1} and CO_2 adsorption capacity of 3294 mg g^{-1} at 318 K and 200 bar. These sulfur COPs also feature high amount of nitrogen and sulfur within the networks which facilitate very high CO_2 adsorption capacity, high temperature stability and selectivity of CO_2 over nitrogen. To the best of our knowledge, sulfur COPs are the first of the sulfur linked nanoporous polymers ever built. Robust, versatile, and inexpensive, this new class of materials will bring functional solids for a wide variety of applications, such as gas capture/separation, lithium ion batteries, solar cells, and supercapacitors.

2. Results and Discussion

Sulfur linked COPs rely on thio-ether, R–S–R bonding. In order to construct these structures, we employed nucleophilic substitutions on a triazine trichloride, commonly known as cyanuric chloride (CC). CC is known to exchange chlorides stepwise by nucleophilic substitutions at different temperatures (**Scheme 1** and Supporting Information Scheme S1).[12] The synthesis of COP–3 follows a typical nucleophilic aromatic substitution by 1,3,5-benzenetrithiol on the highly reactive triazine ring that is destabilized by three chlorides resulting in highly networked insoluble mass. This method proved to be facile (one pot), high yield (85%) and inexpensive, especially devoid of rare metals as catalysts.

The solid state ^{13}C-NMR and ^{1}H-NMR spectra with the assignment of the chemical shifts are presented in **Figure 1**. COP–3 show chemical shifts at 141.6 and 130 ppm, corresponding to the carbons of the aromatic benzene ring. The triazine ring carbons were assigned to 180.6 ppm in the ^{13}C-NMR spectra. In ^{1}H-NMR spectra, chemical shifts at 6.88 and 3.00 ppm correspond to the protons of aromatic benzene and some unreacted terminal aromatic–SH, respectively. Internal standard TMS shows the reference chemical shift at 0 ppm. Functional groups present in COPs show characteristic FTIR absorptions. Several strong bands in the 1200–1600 cm^{-1} region were identified corresponding to the typical stretching modes of CN heterocycles. Additionally, the characteristic breathing mode of the triazine units is evident at 800 cm^{-1}. The absence of the characteristic C–Cl stretching vibration at 850 cm^{-1} confirmed that all three chlorine atoms on cyanuric chloride have been substituted.

TGA of COP–3 was performed up to 800 °C at a heating rate of 10 °C min^{-1} in air and nitrogen environment (Figure 1d). COP–3 is started to decompose at around 340 and 370 °C in air and nitrogen atmosphere, respectively. COP–3 shows superior thermal stability owing to its robust aromatic nature of the framework which is beneficial for considering their potential application in CO_2 scrubbing operations. COP–3 is amorphous as evidenced by their powder X-ray diffraction (XRD) pattern (Supporting Information Figure S1). The phase purity and morphology of COP–3 were investigated by transmission electron microscopy (TEM), which revealed irregular particles with single phase morphology and texture is largely amorphous (Supporting Information Figure S2).

Porosity of COP–3 was confirmed by measuring the Ar adsorption–desorption isotherm at 87 K (**Figure 2**). The fully

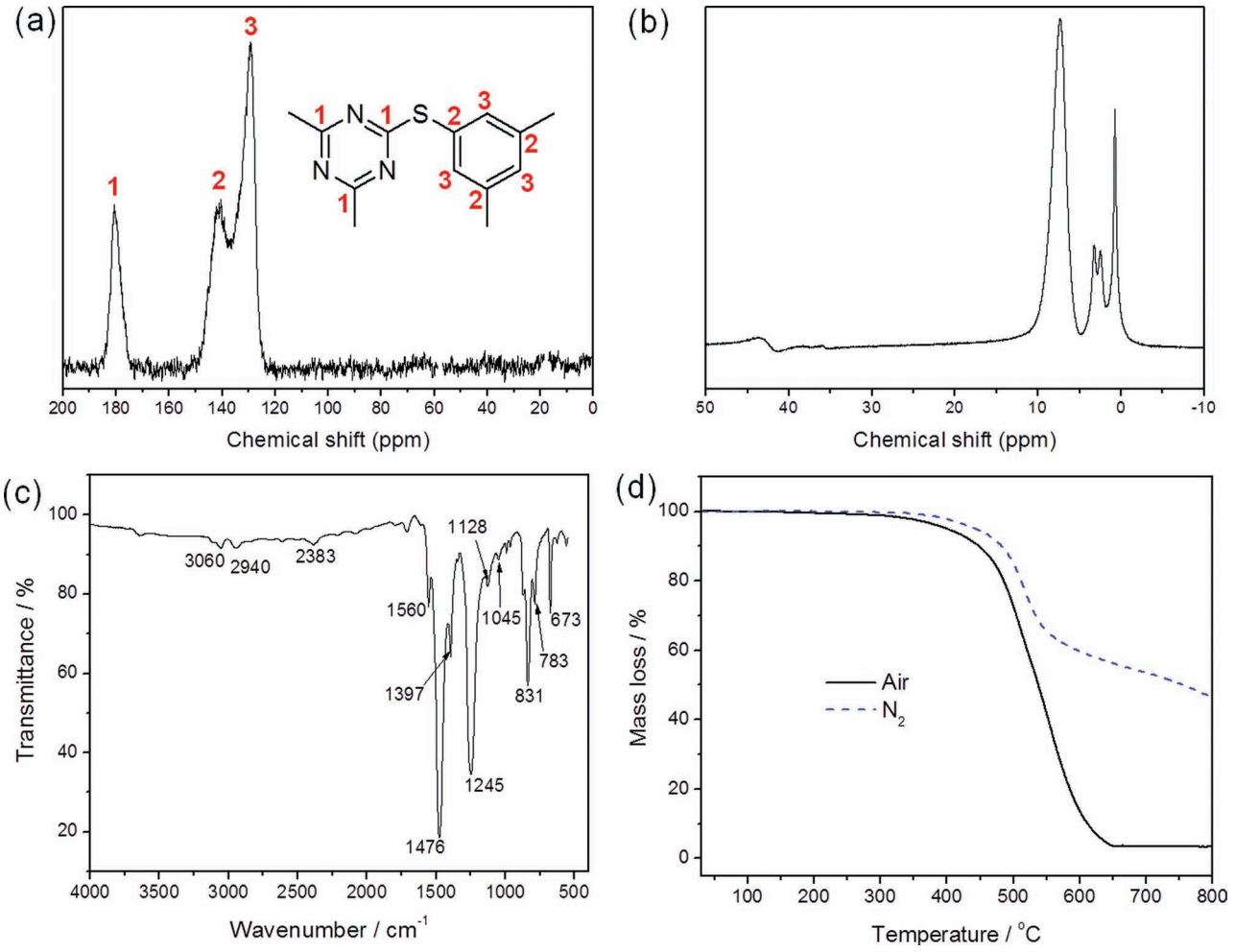

Figure 1. Solid-state a) CP/MAS ^{13}C-NMR spectra, b) ^{1}H-NMR spectra and relative assignments of the respective structures, c) FTIR spectra for COP–3, and d) Thermogravimetric analysis for COP–3 in air and nitrogen.

reversible Type I isotherm shows a rapid uptake at low pressure, 0–0.1 bar, indicating a permanent microporous nature. The gradual increase in Ar uptake and the minor hysteresis may be due to the mesoporosity. The increase in the Ar sorption at relative pressures above 0.9 is due in part from interparticulate porosity associated with the meso- and macro-structures of the samples and inter-particular void. The BET model was applied over the relative pressure range of 0.05–0.25 (Supporting Information Figure S3), which resulted in an apparent BET surface area of 413 m^2 g^{-1}. The Langmuir surface area is found to be 516 m^2 g^{-1}. The average pore size in the micropore region and pore volume calculated from non-local density functional theory (NLDFT) for COP–3 is 2.7 nm and 0.31 cm^3 g^{-1}, respectively. The micropore surface area obtained from NLDFT is 764 m^2 g^{-1} for COP–3. The surface area measured from CO_2 adsorption at 273 K for COP–3 is 310 m^2 g^{-1} (Supporting Information Figure S3).

Interest in CO_2 capture or separation from flue gases or coal-fired plants is highly attractive due to environmental and economic reasons. CO_2 and N_2 sorption isotherms were measured to elucidate the effect of nitrogen-rich framework on the uptake at 273 K and 298 K up to 1 bar (Figure 2b, Supporting Information Table S1). COP–3 shows noteworthy uptakes and the adsorption process is reversible at both temperatures as the desorption branches are very close to that of adsorption. CO_2 capture in COP–3 is due to a combination of microporous and nitrogen-rich framework which results 74 mg g^{-1} and 50 mg g^{-1} CO_2 capture at 273 and 298 K, respectively, at atmospheric pressure. The isosteric heat of adsorption of COP–3 is 24.5 kJ mol^{-1}, in well accordance with nitrogen-rich porous organic frameworks.[28,29] The separation of CO_2 over N_2 is one of the prime requirements for the CO_2 capture technology. N_2 adsorption for COP–3 is 2.8 mg g^{-1} and 2.7 mg g^{-1} at 273 K and 298 K respectively. The selectivity of CO_2 over N_2 was measured by the Henry Law constants from the isotherms in the linear low pressure (<0.1 bar) range (Supporting Information Figure S4). CO_2/N_2 selectivity for COP–3 is 63.7 and 24.4 at 273 and 298 K, at 1 bar which is comparable to reported porous materials.[14,30] The CO_2/N_2 selectivity is also predicted for CO_2:N_2 (0.15:0.85) mixture by ideal adsorbed solution theory (IAST) which shows CO_2/N_2 selectivity of 151 and 107 at 273 and 298 K for COP–3.

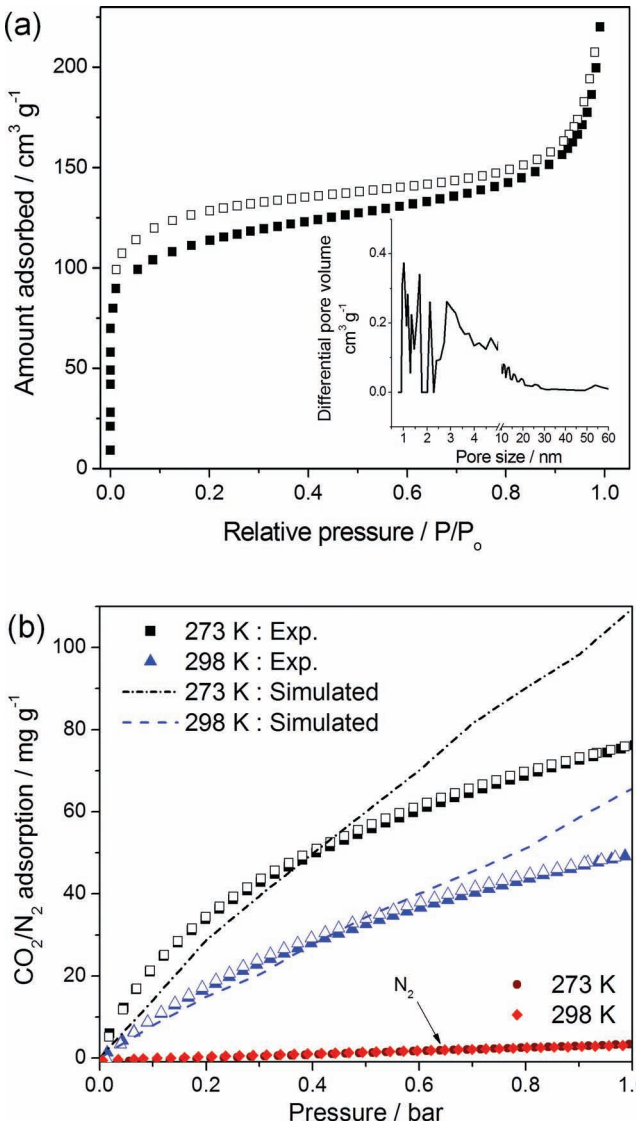

Figure 2. a) Ar adsorption–desorption isotherm measured at 87 K (inset: pore size vs differential pore volume); b) Low pressure CO_2 and N_2 adsorptions for COP–3 at 273 and 298 K up to 1 bar. Adsorption (filled symbols), desorption (open symbols). Theoretical simulation (dashed lines) shows a near fit to the experimental values below 0.5 bar.

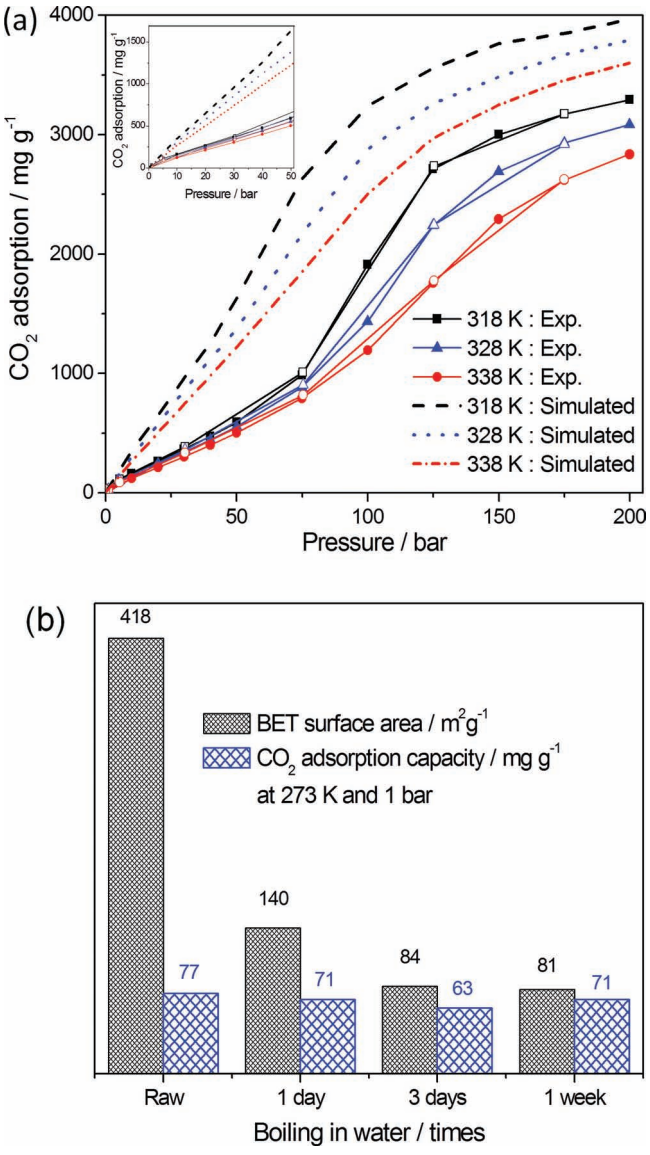

Figure 3. a) High pressure CO_2 adsorptions for COP–3 measure at 318, 328, and 338 K up to 200 bar. CO_2 adsorption (filled symbols)–desorption (open symbols). Theoretical simulated isotherms (dashed lines) show similar shapes and temperature dependency as experimental isotherms. Inset: 0–50 bar region was magnified for better display. b) Effect of boiling in H_2O on BET surface area and low pressure CO_2 adsorption capacities.

High pressure CO_2 adsorption isotherms were collected at 318, 328, and 338 K up to 200 bar to assess the potential of COP–3 for CO_2 capture applications (**Figure 3**, Supporting Information Table S2). Exceptional CO_2 adsorption capacities were obtained at 200 bar, 3294 mg g^{-1} at 318 K, 3085 mg g^{-1} at 328 K and 2836 mg g^{-1} at 338 K. CO_2 isotherms follow a Type IV or V Brunauer isotherm.[31] The simulation results also show the same behavior as the experimental isotherm though the computed absolute values are a bit higher than those of experiment ca. 700 mg g^{-1}. Choi et al.[32] simulated CO_2 capture capacity of three dimensional COFs under high pressure which show Type IV isotherms. Lack of very low pressure saturation by CO_2 for COP–3 leads to isotherm assignments which fall in between Type IV and V. Almost no hysteresis in adsorption–desorption cycle can be attributed to weak interactions between CO_2 and COP–3 frameworks. Indeed polymeric materials are known for their elastic characteristic,[33] leading to an unusual second jump in the high pressure region of CO_2 isotherms which is caused by a reversible flexing effect.[34] Unlike low temperature CO_2 uptake, CO_2 capture capacity under warm conditions is measured to ensure performance of COP–3 in exhaust gas environment. The comparison of COP–3 with some of the established porous polymers and MOFs (Supporting Information

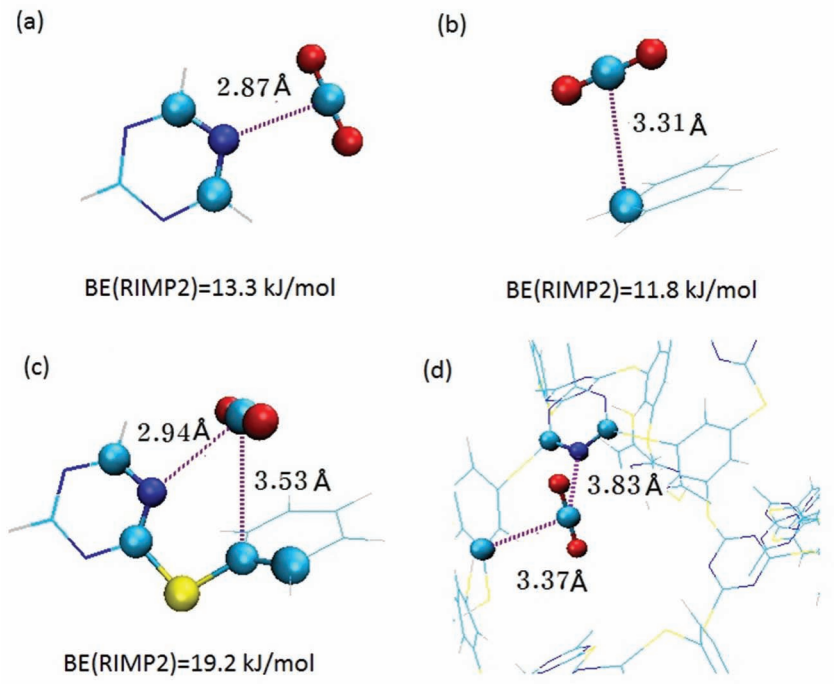

Figure 4. Optimized CO_2 binding configurations for a) 1,3,5-triazine, b) benzene, and c) the sulfur-bridged dimer of the triazine and benzene monomers. In (d), a GCMC snapshot that shows a similar local binding geometry between CO_2 and benzene–triazine dimer motif as in the RIMP2 optimized structure is depicted. A quantitative difference in intermolecular distances between (c) and (d) may be due to a finite temperature effect in GCMC as well as less accurate empirical force field parameters.

Table S3) shows comparable CO_2 uptake at 298 K and 1 bar, however CO_2 uptake exceeds at high pressure for COP–3.

Thermal and water stability of an adsorbent is of prime importance when it is planned to be utilized for adsorption of CO_2 from a fossil fuel burning thermal power plant. COP–3 has been subjected to extreme moist conditions at boiling temperatures to study the stability in steam-like gas streams. For a reliable water stability test, 100–300 mg of COP–3 was dispersed in H_2O (15 mL) and kept at 100 °C for 1 day, 3 days, and 1 week. Samples were drawn after specified time periods, filtered and dried at 100 °C. Their respective surface areas and CO_2 adsorptions were measured (Figure 3b). Although COP–3 lost more than 80% of its BET surface area upon boiling in water, its low pressure CO_2 capacity has not equally degraded which confirms that high surface area is not the desired characteristic for CO_2 uptake.

The GCMC simulations were performed for theoretical comparison of the CO_2 uptake. The polymer model was prepared using the stoichiometric ratio between cyanuric chloride and bezenetrithiol to be 1:1, considering tapped density of COP–3 (0.206 $cm^3\ g^{-1}$). Our GCMC results generally overestimate the CO_2 uptake compared to experiments at high pressures (Figure 3, Supporting Information Table S2 and Table S4), shifted up more or less uniformly, but the shapes of isotherm and their temperature dependence are in reasonable agreement with experiments. A good agreement between theory and experiment is also observed at low pressures below 0.5 bar (Figure 2b). Some deviations in absolute capacities may be due to the FF parameters that are not optimized for this particular system and a limitation of the polymer model used. Quantum chemical investigations of the CO_2 binding geometry and stabilization energy were conducted for 1,3,5-triazine, benzene, and sulfur-bridged dimer of triazine and benzene. M06–2X and RIMP2 yielded the same relative trend of binding energies for monomers and dimers, and here we use RIMP2/aug-cc-pVTZ energetic for discussion. For benzene interacting with CO_2, our results are consistent with previous computations.[11,35] The most stable configurations of the adsorbed complexes are shown in **Figure 4**. Interestingly, the dimer of triazine and benzene plays a cooperative role for a stronger binding of CO_2 (19.2 kJ mol^{-1}) as compared to a separate binding with triazine (13.3 kJ mol^{-1}) or benzene (11.8 kJ mol^{-1}) (Supporting Information Table S5). In 1,3,5-triazine, CO_2 is located on the nitrogen side of aromatic ring in plane whereas for benzene CO_2 goes over the aromatic ring out of plane.

In dimer, the optimized position of CO_2 turns out to be a combination of these two separately optimized structures, namely, interacting both with the side of triazine and top of benzene simultaneously. Indeed, we found that CO_2 preferably interacts with the side of triazine ring where carbon of CO_2 is pointing to nitrogen of triazine. GCMC snapshot that shows a similar local binding geometry as in the RIMP2 lowest energy configuration is depicted in Figure 4d. The relatively longer intermolecular distances between CO_2 and benzene–triazine dimer motif in this GCMC snapshot as compared to RIMP2 may be due to a finite temperature effect in GCMC that simulates experimental conditions unlike QM calculations at 0 K, as well as the use of general FF parameters in GCMC that are not optimal.

Other sulfur based COPs, COP–4, COP–5 and COP–6 were also studied for its low pressure gas adsorption capacity and CO_2/N_2 selectivity (see Supporting Information for their structure and characterizations). The complete substitution of chloride from cyanuric chloride can be seen from FTIR spectrum of COPs 4–6 (Supporting Information Figure S5) confirming formation of sulfur bridged COPs. TGA reveals exceptional thermal stability up to 400 °C for all COPs in nitrogen atmosphere (Supporting Information Figure S6). The specific surface area of COPs 4–6 was quite lower (54 $m^2\ g^{-1}$ for COP–4, 75 $m^2\ g^{-1}$ for COP–5 and 15 $m^2\ g^{-1}$ for COP–6) than COP–3 as shown in **Figure 5**a and Supporting Information Figure S7. It is clearly visible that these COPs are not containing microporous network and show large pores, mainly arises from macroporosity. The BET surface area is also calculated from CO_2 isotherms at 273 K, indicating 269.6 $m^2\ g^{-1}$ for COP–4, 120.3 $m^2\ g^{-1}$ for COP–5 and 106.7 $m^2\ g^{-1}$ for COP–6. CO_2 capture capacity (Figure 5b, Supporting Information Table S1) of COPs 4–5 ranges from 24–33 mg g^{-1} at 273 K and 1 bar which is mainly due to presence of nitrogen-rich frameworks. CO_2/N_2

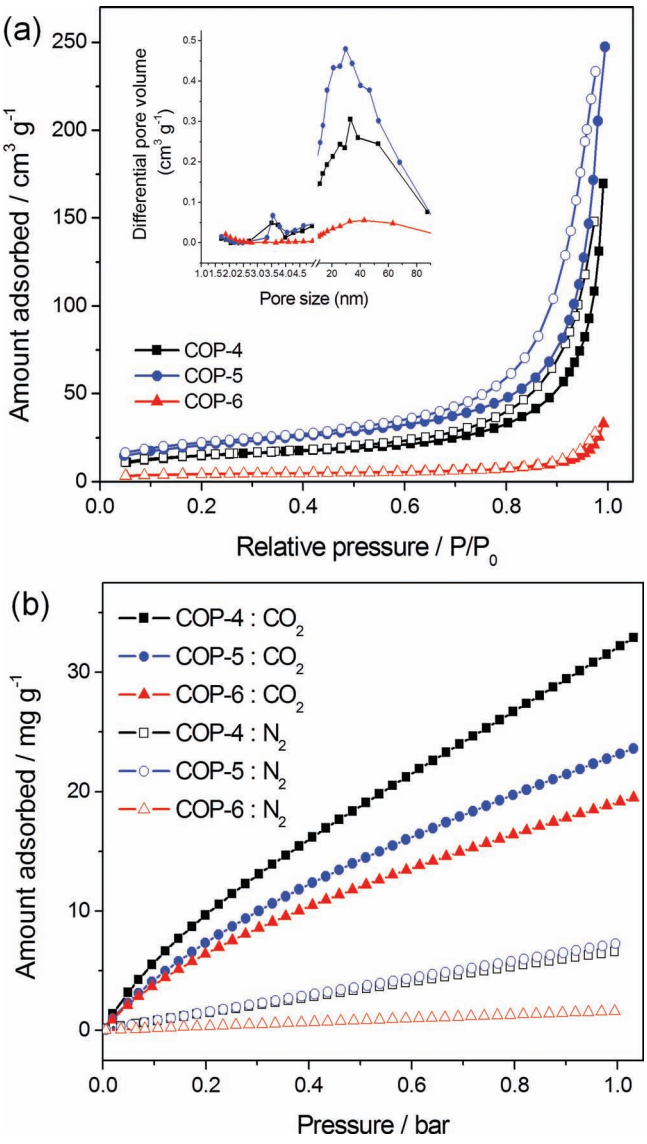

Figure 5. a) N_2 adsorption–desorption isotherm for COPs 4–6 measured at 77 K (inset: pore size vs pore volume); b) Low pressure CO_2 and N_2 adsorptions for COPs 4–6 at 273 K up to 1 bar. Adsorption (filled symbols), desorption (open symbols).

selectivity of COPs 4–6 measured by Henry's constant is very poor, 8.1 for COP–4, 5.3 for COP–5 and 22 for COP–6 (Supporting Information Figure S8 and Table S1), ranging from 3.3–12.5 suggesting that COPs 4–5 does not have much potential for gas separation applications. This is further confirming by predicting CO_2:N_2 gas mixture selectivity by IAST which show 24.8 for COP–4, 18.1 for COP–5 and 65.8 for COP–6.

3. Conclusions

First sulfur bridged, nitrogen-rich, nanoporous covalent organic polymers (COPs) were synthesized by controlled nucleophilic substitution of cyanuric chloride and investigated for porosity and gas uptake under various conditions. COP–3 exhibits moderate surface areas however COP–3 shows exceptional CO_2 capacity at 200 bar, even in the warm conditions. CO_2/N_2 selectivities and isosteric heat of adsorption of COP–3 is on par with nitrogen-rich porous polymers, while being superior in stability. Although surface area of COPs 4–6 is very low, it shows moderate low pressure CO_2 sorption capacity.

4. Experimental Section

Materials: Cyanuric chloride and *N,N*-diisopropylethylamine (DIPEA) were purchased from Sigma-Aldrich, USA. 1,3,5-benzenetrithiol, 1,4-benzenedithiol, biphenyl-4,4′-dithiol, 4,4′-thiobisbenzenethiol were obtained from TCI, Japan. 1,4-dioxane and ethyl alcohol were purchased from SAMCHUN, South Korea. All solvents were dried and stored in anhydrous conditions.

Synthesis of Sulfur COPs: In a typical synthesis, DIPEA (2.5 mL, 14.3 mmol) was added to 1,3,5-benzenetrithiol (0.52 g, 3.0 mmol) dissolved in 1,4-dioxane (120 mL) at 15 °C. Cyanuric chloride (0.50 g, 2.7 mmol), dissolved in 1,4-dioxane (30 mL), was added dropwise to the above solution with continuous stirring at 15 °C in an N_2 environment. The yellowish white precipitate was stirred at 15 °C for 1 h before being stirred at 25 °C for 2 h and then at 85 °C for 21 h. The white precipitate was washed with 1,4-dioxane and soaked in ethyl alcohol three times over the period of 12 h. Finally, the precipitate was dried at room temperature under vacuum for 2 h. Yield: 85%. Elemental analysis for $C_9N_3H_3S_3$ calculated (%): C, 43.4; H, 1.2; N, 16.8 and found (%): C, 44.6; H, 1.7; N, 14.6. This sample is designated as COP–3 following the order after our previous report on COPs.[12] A typical pathway for the substitution of chloride of cyanuric chloride at different temperature is demonstrated in Supporting Information Scheme S1. COPs 4–6 were synthesized following a similar procedure (see Supporting Information for further details).

Characterization: ^1H and ^{13}C NMR spectra were recorded on a Bruker DMX400 NMR spectrometer. Solid-state cross polarization magic angle spinning (CP/MAS) NMR spectra was taken by a Bruker Anence III 400 WB NMR spectrometer. FTIR spectra were obtained on KBr pellets using a Perkin–Elmer FT-IR spectrometer. Thermogravimetric analysis (TGA) was performed on a NETZSCH–TG 209 F3 instrument by heating the samples to 800 °C at 10 °C min^{-1} in N_2 or air atmosphere. CHNS analyses were done on elemental analyzer ThermoQuest Italia S.P.A (CE Instrument). Ar sorption isotherms were obtained with a Micromeritics ASAP 2020 accelerated surface area and porosimetry analyzer at 87 K. Prior to analysis, the samples were degassed at 150 °C for 5 h under vacuum. The adsorption–desorption isotherms were evaluated to give the pore parameters, including Brunauer–Emmett–Teller and Langmuir surface area, pore size and pore volume.[36] The pore size distribution and micropore surface area was determined by non-local density functional theory (NLDFT). X-ray diffraction (XRD) patterns of the samples were acquired from 0.5° to 60° by a Rigaku D/MAX–2500 (18kW) micro-area X-ray diffractometer.

Low and High Pressure Gas Adsorption: The low pressure CO_2 and N_2 adsorption–desorption isotherms were measured separately at 273 K using a static volumetric system (ASAP 2020, Micromeritics Inc.). The temperature during adsorption and desorption was kept constant using a circulator. Prior to adsorption measurements, the samples were activated in situ by increasing the temperature at a heating rate of 1 K min^{-1} up to 423 K under vacuum (5×10^{-3} mmHg) and maintained for 5 h before the sorption measurements. Isosteric heats of adsorption were calculated from the adsorption data using Clausius–Clapeyron equation,[37]

$$\Delta_{ad}H^{\circ} = R\left[\partial \ln P \Big/ \partial\left(1/T\right)\right]_{\theta}$$

where, R is the universal gas constant, θ is the fraction of the adsorbed sites at a pressure P and temperature T. The CO_2/N_2 selectivity was calculated from Henry's constant and ideal adsorbed solution theory (IAST).[38] Rubotherm Magnetic Suspension Balance (MSB) was utilized for high pressure CO_2 adsorption capacity determination. In a typical

high pressure CO_2 adsorption–desorption isotherm measurement, approximately 0.25 g of COP–3 was placed on a holder that was previously activated at 423 K. The system is taken under vacuum for 24 h at 336 K. CO_2 is pressurized via Teldyne Isco 260D fully automated gas booster and charged into the high pressure cell. CO_2 adsorption–desorption isotherms at 318, 328, and 338 K up to 200 bar were measured.[12,33,39]

Simulation Methods: Theoretical CO_2 capacities were determined using grand canonical Monte Carlo (GCMC) simulations with the Cerius2 v. 4.0 software. The force field (FF) parameters and charges for CO_2 were adopted from Harris et al.[40] and those for COP–3 were obtained from Dreiding 2.21 and equilibrium charge method. The amorphous polymer COP–3 was prepared using an amorphous builder in Cerius2. Quantum mechanical (QM) calculations of the binding energy of CO_2 with 1,3,5-triazine, benzene, and a sulfur-bridged triazine-benzene dimer were performed using Q-CHEM.[41] The B3LYP, M06-2X and RIMP2 calculations using the cc-pVTZ//6-31G* basis (geometry optimization with the 6-31G* basis followed by single point energy calculations with cc-pVTZ) were performed, and counterpoise correction for basis set superposition error was included. To see the effects of adding diffuse functions, RIMP2 energetics were refined with the aug-cc-pVTZ basis using dual basis method.[42]

Supporting Information

Supporting Information is available from the Wiley Online Library or from the author.

Acknowledgements

This work was made possible by NPRP grant # 08–670–1–124 from the Qatar National Research Fund (a member of Qatar Foundation). The statements made herein are solely the responsibility of the authors. We also acknowledge the financial support by grants from Korea CCS R&D Center, IWT (NRF-2012-C1AAA001-M1A2A2026588) and WCU program (R31-2008-000-10055-0), funded by the Ministry of Education, Science and Technology of Korean government, and KAIST EEWS Initiative.

Received: August 27, 2012
Revised: October 24, 2012
Published online: December 17, 2012

[1] R. Dawson, A. I. Cooper, D. J. Adams, *Prog. Polym. Sci.* **2011**, *37*, 530.
[2] A. Thomas, *Angew. Chem. Int. Ed.* **2010**, *49*, 8328.
[3] A. P. Cote, A. I. Benin, N. W. Ockwig, M. O'Keeffe, A. J. Matzger, O. M. Yaghi, *Science* **2005**, *310*, 1166.
[4] S. Wan, F. Gandara, A. Asano, H. Furukawa, A. Saeki, S. K. Dey, L. Liao, M. W. Ambrogio, Y. Y. Botros, X. F. Duan, S. Seki, J. F. Stoddart, O. M. Yaghi, *Chem. Mater.* **2011**, *23*, 4094.
[5] F. Karadas, H. El-Faki, E. Deniz, C. T. Yavuz, S. Aparicio, M. Atilhan, *Microporous Mesoporous Mater.* **2012**, *162*, 91.
[6] R. E. Morris, P. S. Wheatley, *Angew. Chem. Int. Ed.* **2008**, *47*, 4966.
[7] D. M. D'Alessandro, B. Smit, J. R. Long, *Angew. Chem. Int. Ed.* **2010**, *49*, 6058.
[8] M. J. Rosseinsky, *Microporous Mesoporous Mater.* **2004**, *73*, 15.
[9] O. K. Farha, J. T. Hupp, *Acc. Chem. Res.* **2010**, *43*, 1166.
[10] J. Seo, H. Sakamoto, R. Matsuda, S. Kitagawa, *J. Nanosci. Nanotechnol.* **2010**, *10*, 3.
[11] J. Park, H. Kim, S. S. Han, Y. Jung, *J. Phys. Chem. Lett.* **2012**, *3*, 826.
[12] H. A. Patel, F. Karadas, A. Canlier, J. Park, E. Deniz, Y. Jung, M. Atilhan, C. T. Yavuz, *J. Mater. Chem.* **2012**, *22*, 8431.
[13] P. Mohanty, L. D. Kull, K. Landskron, *Nat. Commun.* **2011**, *2*, 1.
[14] R. Dawson, E. Stockel, J. R. Holst, D. J. Adams, A. I. Cooper, *Energy Environ. Sci.* **2011**, *4*, 4239.
[15] D. Yuan, W. Lu, D. Zhao, H.-C. Zhou, *Adv. Mater.* **2011**, *23*, 3723.
[16] T. Ben, H. Ren, S. Q. Ma, D. P. Cao, J. H. Lan, X. F. Jing, W. C. Wang, J. Xu, F. Deng, J. M. Simmons, S. L. Qiu, G. S. Zhu, *Angew. Chem. Int. Ed.* **2009**, *48*, 9457.
[17] A. P. Katsoulidis, M. G. Kanatzidis, *Chem. Mater.* **2011**, *23*, 1818.
[18] W. Lu, J. Sculley, D. Yuan, R. Krishna, Z. Wei, H. C. Zhou, *Angew. Chem. Int. Ed.* **2012**, *51*, 1.
[19] N. B. McKeown, P. M. Budd, *Chem. Soc. Rev.* **2006**, *35*, 675.
[20] N. B. McKeown, P. M. Budd, *Macromolecules* **2010**, *43*, 5163.
[21] P. M. Budd, N. B. McKeown, *Polym. Chem.* **2010**, *1*, 63.
[22] N. B. McKeown, P. M. Budd, in *Porous Polymers* (Eds: M. S. Silverstein, N. R. Cameron, M. A. Hillmyer), John Wiley & Sons, Inc., New York **2011**, Ch. 1.
[23] M. B. Steffensen, E. E. Simanek, *Org. Lett.* **2003**, *5*, 2359.
[24] A. Thomas, A. Fischer, F. Goettmann, M. Antonietti, J. O. Muller, R. Schlogl, J. M. Carlsson, *J. Mater. Chem.* **2008**, *18*, 4893.
[25] J. P. Paraknowitsch, J. Zhang, D. S. Su, A. Thomas, M. Antonietti, *Adv. Mater.* **2010**, *22*, 87.
[26] A. Fischer, J. O. Muller, M. Antonietti, A. Thomas, *ACS Nano* **2008**, *2*, 2489.
[27] H. Y. Zhao, Z. Jin, H. M. Su, X. F. Jing, F. X. Sun, G. S. Zhu, *Chem. Commun.* **2011**, *47*, 6389.
[28] A. Laybourn, R. Dawson, R. Clowes, J. A. Iggo, A. I. Cooper, Y. Z. Khimyak, D. J. Adams, *Polym. Chem.* **2012**, *3*, 533.
[29] M. G. Rabbani, H. M. El-Kaderi, *Chem. Mater.* **2011**, *23*, 1650.
[30] M. G. Rabbani, H. M. El-Kaderi, *Chem. Mater.* **2012**, *24*, 1511.
[31] D. M. Ruthven, *Principles of Adsorption and Adsorption Processes*, John Wiley & Sons, Inc., New York **1984**.
[32] Y. J. Choi, J. H. Choi, K. M. Choi, J. K. Kang, *J. Mater. Chem.* **2011**, *21*, 1073.
[33] S. Zulfiqar, F. Karadas, J. Park, E. Deniz, G. D. Stucky, Y. Jung, M. Atilhan, C. T. Yavuz, *Energy Environ. Sci.* **2011**, *4*, 4528.
[34] D. Tanaka, A. Henke, K. Albrecht, M. Moeller, K. Nakagawa, S. Kitagawa, J. Groll, *Nat. Chem.* **2010**, *2*, 410.
[35] M. Besnard, M. I. Cabaco, D. Talaga, Y. Danten, *J. Chem. Phys.* **2008**, *129*, 224511.
[36] C. T. Yavuz, J. Mayo, C. Suchecki, J. Wang, A. Ellsworth, H. D'Couto, E. Quevedo, A. Prakash, L. Gonzalez, C. Nguyen, C. Kelty, V. Colvin, *Environ. Geochem. Health* **2010**, *32*, 327.
[37] R. R. Pawar, H. A. Patel, G. Sethia, H. C. Bajaj, *Appl. Clay Sci.* **2009**, *46*, 109.
[38] W. Lu, J. P. Sculley, D. Yuan, R. Krishna, Z. Wei, H.-C. Zhou, *Angew. Chem. Int. Ed.* **2012**, *51*, 1.
[39] F. Karadas, C. T. Yavuz, S. Zulfiqar, S. Aparicio, G. D. Stucky, M. Atilhan, *Langmuir* **2011**, *27*, 10642.
[40] J. G. Harris, K. H. Yung, *J. Phys. Chem.* **1995**, *99*, 12021.
[41] Y. Shao, L. F. Molnar, Y. Jung, J. Kussmann, C. Ochsenfeld, S. T. Brown, A. T. B. Gilbert, L. V. Slipchenko, S. V. Levchenko, D. P. O'Neill, R. A. DiStasio, R. C. Lochan, T. Wang, G. J. O. Beran, N. A. Besley, J. M. Herbert, C. Y. Lin, T. Van Voorhis, S. H. Chien, A. Sodt, R. P. Steele, V. A. Rassolov, P. E. Maslen, P. P. Korambath, R. D. Adamson, B. Austin, J. Baker, E. F. C. Byrd, H. Dachsel, R. J. Doerksen, A. Dreuw, B. D. Dunietz, A. D. Dutoi, T. R. Furlani, S. R. Gwaltney, A. Heyden, S. Hirata, C. P. Hsu, G. Kedziora, R. Z. Khalliulin, P. Klunzinger, A. M. Lee, M. S. Lee, W. Liang, I. Lotan, N. Nair, B. Peters, E. I. Proynov, P. A. Pieniazek, Y. M. Rhee, J. Ritchie, E. Rosta, C. D. Sherrill, A. C. Simmonett, J. E. Subotnik, H. L. Woodcock, W. Zhang, A. T. Bell, A. K. Chakraborty, D. M. Chipman, F. J. Keil, A. Warshel, W. J. Hehre, H. F. Schaefer, J. Kong, A. I. Krylov, P. M. W. Gill, M. Head-Gordon, *Phys. Chem. Chem. Phys.* **2006**, *8*, 3172.
[42] R. A. Distasio, R. P. Steele, M. Head-Gordon, *Mol. Phys.* **2007**, *105*, 2731.